energies

MDPI

Article

Multi-Objective Optimization of the Energy, Exergy, and Environmental Performance of a Hybrid Solar–Biomass Combined Brayton/Organic Rankine Cycle

Guillermo Valencia-Ochoa [1,*], Jorge Duarte-Forero [1] and Daniel Mendoza-Casseres [2]

[1] Programa de Ingeniería Mecánica, Universidad del Atlántico, Carrera 30 Número 8-49, Puerto Colombia, Barranquilla 080007, Colombia; jorgeduarte@mail.uniatlantico.edu.co
[2] Programa de Ingeniería Industrial, Universidad del Atlántico, Carrera 30 Número 8-49, Puerto Colombia, Barranquilla 080007, Colombia; danielmendoza@mail.uniatlantico.edu.co
* Correspondence: guillermoevalencia@mail.uniatlantico.edu.co; Tel.: +57-324-94-31

Abstract: This research proposes integrating a combined system from a supercritical Brayton cycle (SBC) at extremely high temperatures and pressures and a conventional ORC cycle. The ORC cycle was evaluated with three working fluids: acetone, toluene, and cyclohexane. Of these, the cyclohexane, thanks to its dry fluid condition, obtained the best result in the sensitivity analysis for the energetic and exergetic evaluations with the most relevant (net power and exergy destruction) for the variation in the most critical performance parameter of the system for both the configuration with reheat and the configuration with recompression. Between the two proposed configurations, the most favorable performance was obtained with a binary system with reheat and recompression; with reheat, the SBC obtained first- and second-law efficiencies of 45.8% and 25.2%, respectively, while the SBC obtained values of 54.8% and 27.9%, respectively, with reheat and recompression. Thus, an increase in overall system efficiency of 30.3% is obtained. In addition, the destroyed exergy is reduced by 23% due to the bypass before the evaporation process. The SBC-ORC combined hybrid system with reheat and recompression has a solar radiation of 950 W/m^2 K, an exhaust heat recovery efficiency of 0.85, and a turbine inlet temperature of 1008.15 K. The high pressure is 25,000 kPa, the isentropic efficiency of the turbines is 0.8, the pressure ratio is 12, and the pinch point of the evaporator is initially 20 °C and reaches values of 45 °C in favorable supercritical conditions.

Keywords: simulation; cycle; ORC; SBC; superheat; pinch point; recompression

Academic Editor: George Kosmadakis

Received: 30 November 2024
Revised: 27 December 2024
Accepted: 31 December 2024
Published: 6 January 2025

Citation: Valencia-Ochoa, G.; Duarte-Forero, J.; Mendoza-Casseres, D. Multi-Objective Optimization of the Energy, Exergy, and Environmental Performance of a Hybrid Solar–Biomass Combined Brayton/Organic Rankine Cycle. *Energies* **2025**, *18*, 203. https://doi.org/10.3390/en18010203

1. Introduction

Energy consumption for electricity generation has significantly increased today [1]. This increase has also increased carbon emissions due to the continued use of fossil fuels. However, reserves of these resources are steadily decreasing, posing the growing challenge of identifying energy sources that are both reliable and sustainable [2]. The serious environmental problems caused by using fossil fuels have accelerated the use of renewable energies [3]. Biomass, wind, solar, and geothermal energy represent some of the main renewable sources used today to generate clean and environmentally friendly energy [4]. Some studies propose the investigation of energy scheduling methods using renewable energy sources, such as solar energy and biomass, in order to simulate energetically and economically the demands for electricity, heat, and irrigation [5]. Solar energy is considered the main source of renewable energy that reduces the demand for fossil fuels [6]. This

is particularly important because of the need to control global warming and meet the growing electricity demand. Sunlight can be used for heating and power generation by capturing solar collectors. These devices are required to reach high temperatures, and their configurations include parabolic trough collectors, disk collectors, and heliostats, among others. Temperature ranges are wide, reaching ranges of 150–1500 °C (heliostats), 750–1000 °C (disk collectors), and 60–500 °C (parabolic trough collectors) [7]. Solar energy can be used for electricity generation through technologies such as photovoltaic (PV) cells and concentrating solar power (CSP) systems [8]. The former (photovoltaic power plants) are suitable for installation in specific areas with sufficient sunlight or far from renewable energy sources [9]. On the other hand, CSP uses concentrated solar radiation to activate a thermodynamic cycle [10]. Among the various CSP technologies, solar tower power plants (STPPs) have attracted attention in recent years. In STPPs, an array of flat mirrors (heliostats) can reflect sunlight back to a central receiver, resulting in extremely high temperatures. This allows coupling with conventional generation systems such as the organic Rankine cycle [11].

In recent years, various investigations have been carried out focused on evaluating the operational aspects of STPPs. These investigations include the analysis of the types of receivers, the distribution of heliostat fields, and power generation units, among others, which aim to improve power generation and achieve greater efficiency [12]. Zhou et al. [13] proposed a combined cycle based on a supercritical Brayton cycle using helium as the working fluid. The proposed cycle combines the conventional Brayton cycle with the organic Rankine cycle and an absorption chiller for waste heat recovery. For the optimal conditions, an increase in energy efficiency of 14.5% and a reduction in electricity cost of 11.9% in the combined cycle was obtained. Khan et al. [14] investigated a cycle formed by a helium Brayton cycle and a transcritical CO_2 cycle for waste heat recovery. The proposed combined cycle achieved a thermal efficiency of 32.39% and an exergy efficiency of 34.68%. In general, the exergy and energy efficiency of the combined cycle allowed increases of 13.18% and 13.21%, respectively. Additionally, a 2% reduction in the cost of the electricity produced was obtained. Khan et al. [15] evaluated a combined cycle for a solar power plant composed of a helium Brayton cycle and a medium-temperature organic Rankine cycle for waste heat recovery. The conclusions indicate an improvement in energy efficiency of 19.11%. The proposed cycle achieves an exergy and energy efficiency of 39.74% and 37.11%. Etghani et al. [16] proposed a system consisting of a parabolic trough collector, recuperative organic Rankine cycle (RORC), supercritical CO_2 Brayton cycle (SCBC), direct thermal energy storage system, and proton exchange membrane electrolyzer. It was observed that the system could generate 1.5 MW of net power, with an efficiency of 33.89% in the solar collector.

In most industrial and power generation processes, the fundamental principles of heat transfer between fluids have been applied to take advantage of the available energy in the form of heat present during the interaction of a cold fluid and a hot fluid [17]. However, these processes present many losses and environmental impacts due to the release of waste gases, which can be used to recover energy within the system [18]. Hou et al. [19] performed the optimization of a combined cycle system consisting of a supercritical CO_2 recompression cycle and a regenerative cycle to improve the part-load thermal efficiency of a ship from the waste heat recovery of marine gas turbines. Finally, the proposed cycle improves the part-load efficiency of the ship since it allows it to reach 80% of the required propulsion power when the gas turbine fails, thanks to the recovered heat. In addition, studies by M. Osagie et al. [20] explore different working fluids in combined cycles added to the Rankine cycle (ORC) and thus propose that of the different fluids studied, the R-123 fluid has the highest energy efficiency of approximately 70%, which

makes the process profitable. Chammam et al. [21] investigated a multigeneration system to produce electricity, cooling, and fresh water. The study focused on parametric analysis and the evaluation of the effect of design variables on energy efficiency and total cost. An energy efficiency of 70.2% was achieved at the optimum operating point. Khaliq et al. [22] proposed a new central receiver design to improve the solar energy-to-heat conversion rate. The research development involved using energy and exergy modeling for the combined power and cooling system. The findings show that the change in ORC working fluid type largely influences the system performance.

Concentrated solar power technology plays a key role in solving the challenge of power generation in tropical countries, both now and in the future, by harnessing the availability of solar heat [23]. The Caribbean region is in northern Colombia and covers an area of 132,270.5 km^2, equivalent to 11.6% of Colombian territory, which makes it a large region with biogeographic diversity [24]. The region has essential air and sun indicators, as the Ministry of Mines and Energy reported, which affirms that it has a high potential for inexhaustible energy utilization. Thus, the region has the resources to become an excellent energy generator from non-conventional sources, favoring the environment due to non-polluting energy sources [25]. The energy potential of the Caribbean region has been the subject of research for many years. Ospino et al. [26] conducted a study of the technical and economic feasibility of implementing photovoltaic renewable systems by selecting the appropriate area using technology according to the conditions of the Caribbean region. The research affirms that across the Colombian national territory, there is a multiannual daily average of about 4.5 kWh/m^2 of usable solar energy, which provides great opportunities to meet the energetic requirements of the country. Likewise, other research performed by J. Gómez et al. [27] shows that, thanks to Colombia's geographic location, it has a high level of solar radiation power whose use could supply the country's electricity demands.

Therefore, the main contribution of this research is the scarcity of studies on the implementation of generation systems to supply the energy demand in different locations of the Colombian Caribbean region with high energy resources. The causes that generated this problem are the scarcity of research; the lack of knowledge of the energy, exergy, and environmental performance; and the low utility in the application of hybrid thermodynamic cycles. The effects identified from this problem are limited thermodynamic cycles, low applicability in hybrid systems of combined thermodynamic cycles, and inefficiency in supplying the energy demand.

2. Methodology

This section presents the fundamental equations for thermodynamic modeling based on the energetic and exergetic designs of the hybrid system with the Brayton/ORC combined cycle. MATLAB software vR2024a was the tool used to simulate the algorithm to solve the proposed equations; in addition, the NIST REFPROP library of organic fluids was used to study the dynamics of the process under several scenarios with different working fluids in the system. This methodology was also implemented to select biomass and organic fluids for the modeling.

This research proposes using solar energy and biomass as a combined heat source in the power supply of a Brayton/ORC combined cycle for electric power generation. Furthermore, the inference of the organic working fluid on the performance of the combined cycle is studied using the energetic and exergetic indicators of the overall system.

2.1. Description and Operation of the System

The hybrid generation system consists of two pieces of equipment that are ideal for energy capture and conversion: solar collectors and the biomass burner. The brine is used

to transport fluid or thermal fluid through the thermodynamic interaction inside the heater (HR), which is then driven by Pump 2 (P2) with controlled flow (gate valves are added for fluid routing) back to the heat source. The sources can be programmed to operate in duality, which increases the energy transfer to the heat transfer fluid. However, renewable sources can be efficient under certain conditions when operating in singularity.

The brine is sent to increase the CO_2 temperature to supercritical conditions with high pressure and temperature, with this regime entering (Stream 1) into Turbine 1 (T1), where it expands and generates work. Thereafter, the output stream from T1 (Stream 2) is supplied to a Re-Heater (RHR) to increase its temperature again to the cycle temperature. The fluid that leaves RHR (current 3) supplies Turbine 2 (T2), which rotates the generator and is coupled to its shaft to generate electrical energy. The stream leaving T2 (Stream 4) passes through the High-Temperature Recuperator (HTR), where CO_2 decreases its temperature by giving up part of its heat to the stream coming from the compression. At this stage, it is proposed that the performance of two different configurations be evaluated to improve the overall efficiency of the SBC by increasing the CO_2 temperature in the stream that enters the HTR and initiates the overall cycle.

Both proposed systems use an ORC cycle to capture the waste heat from the exhaust gases in the turbines that make up the supercritical Brayton cycles. This other cycle is operated in the same mode for both configurations, with a fluid that is transported by Pump 1 (P1) to the evaporator, where it is heated to enter Turbine 3 (T3), which expands the fluid by rotating an electric generator coupled to the shaft; at this stage, the fluid goes through a cooling and condensation process before entering P_1 through a stream of cold water, thus starting the ORC cycle again.

The Brayton/ORC configuration with reheat (refer to Figure 1) initiates with Stream 5, leaving the HTR for the evaporator, where it gives up heat to the ORC cycle before entering the cooler (Stream 5a); at this time, the CO_2 is cooled by a cold air stream coming from the outside (Streams 9 and 10) and is directed (Stream 6) to Compressor 1 (C1), which increases the isentropic pressure of the fluid, before reaching the HTR (Stream 7), where the CO_2 is preheated as the preparation of the SBC using the residual heat of the exhaust gases at T2, thus initiating the last stage of the fluid entering the HR (Stream 8) and closing the cycle.

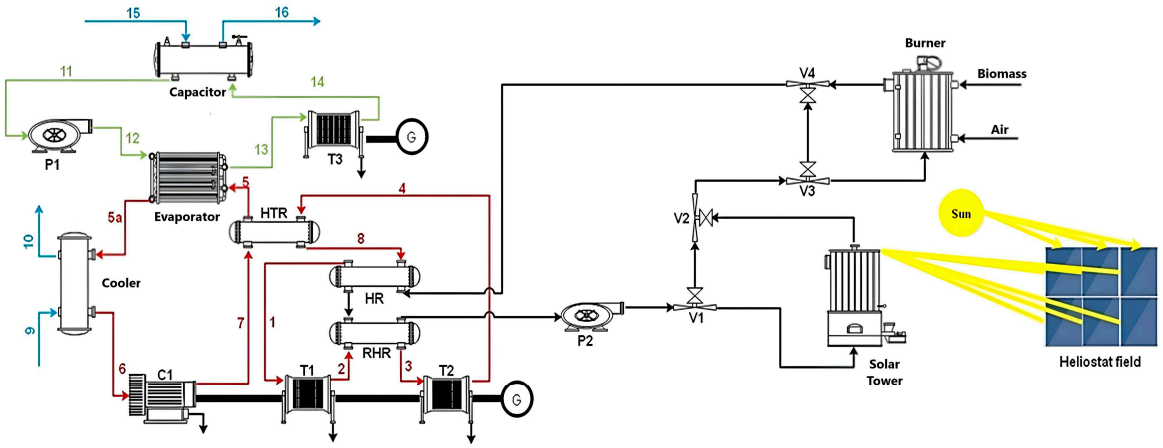

Figure 1. Diagram of the hybrid system with superheating.

The system with recompression adds a bypass to the outlet (Stream 6) of the Low-Temperature Recuperator (LTR) that splits a fraction of the CO_2 to a secondary compressor (C_2) before the remaining working fluid (Stream 6a) enters the precooling process and the fraction of the flow that was sent is pressurized by C_2 and reintroduced between HTR and LTR. Due to the immediate change in CO_2 properties near the critical point, the cold stream has a higher specific heat than the hot fluid.

2.2. Fundamental Equations

For the study of the system, energetic and exergy modeling is carried out under a modular approach in which each component is studied individually, where the effect of each one on the overall behavior of the system is analyzed.

$$\Sigma \dot{m}_{inlet} - \Sigma \dot{m}_{output} = \frac{dm}{dt} \quad (1)$$

The energy balance in the control volume is given by the difference between the energy variation at the input and output, which is equal to the sum of the heat transferred and the power generated in the control volume.

$$\sum \dot{m}_{inlet} h_{inlet} - \sum \dot{m}_{output} h_{output} - \sum \dot{Q} + \sum \dot{W} = \frac{dE}{dt} \quad (2)$$

The balances allow modeling the behavior of the performance variables by applying the main formulas in each piece of equipment that makes up the system. Table 1 shows the formulas designed in the design algorithm for calculating the equipment's thermodynamic properties.

Table 1. Fundamental equations of the hybrid system components.

Components	Symbol	Equation	
Pump 1	P1	$\dot{W}_{P1} = \dot{m}_{ORC}(h_{12} - h_{11})$	(3)
		$\eta_{P1} = \frac{v_{11}(P_{12} - P_{11})}{h_{12} - h_{11}}$	(4)
Pump 2	P2	$\dot{W}_{P2} = \dot{m}_s(h_{s3} - h_{s2})$	(5)
		$\eta_{P2} = \frac{v_s(P_{s3} - P_{s2})}{h_{s3} - h_{s2}}$	(6)
Heat Recovery	HR	$\dot{Q_{HR}} = \dot{m}_s(h_{s0} - h_{s1}) = \dot{m}_{SBC}(h_1 - h_8)$	(7)
Re-Heat Recovery	RHR	$\dot{Q_{RHR}} = \dot{m}_s(h_{s1} - h_{s2}) = \dot{m}_{SBC}(h_3 - h_2)$	(8)
High Temperature Recuperator	HTR	$\dot{Q_{HTR}} = (h_7 - h_8) = (h_5 - h_4)$	(9)
Evaporator Zone 1: Pre-heat Zone 2: Evaporation Zone 3: Overheat	-	$\dot{Q_{prec}} = \dot{m}_{SBC}(h_{liq5} - h_{5a}) = \dot{m}_{ORC}(h_{liq12} - h_{12})$	(10)
		$\dot{Q_{evap}} = \dot{m}_{SBC}(h_{gas5} - h_{liq5}) = \dot{m}_{mez} h_{evap\_ORC}$	(11)
		$\dot{Q_{sob}} = \dot{m}_{SBC}(h_5 - h_{gas5}) = \dot{m}_{ORC}(h_{13} - h_{gas12})$	(12)
Cooler	-	$\dot{Q_{cool}} = \dot{m}_{SBC}(h_{5a} - h_6) = \dot{m}_{aire}(h_{10} - h_9)$	(13)
Compressor 1	-	$\dot{W}_{C1} = \dot{m}_{SBC}(h_7 - h_6)$	(14)
		$\eta_{C1} = \frac{v_6(P_7 - P_6)}{h_7 - h_6}$	(15)
Turbine 1	T1	$\dot{W}_{T1} = \dot{m}_{SBC}(h_1 - h_2)$	(16)
		$\eta_{T1} = \frac{h_1 - h_2}{h_1 - h_{2s}}$	(17)
Turbine 2	T2	$\dot{W}_{T2} = \dot{m}_{SBC}(h_3 - h_4)$	(18)
		$\eta_{T2} = \frac{h_3 - h_4}{h_3 - h_{4s}}$	(19)
Turbine 3	T3	$\dot{W}_{T3} = \dot{m}_{ORC}(h_{13} - h_{14})$	(20)
		$\eta_{T3} = \frac{h_{13} - h_{14}}{h_{13} - h_{14s}}$	(21)
Condenser	-	$\dot{Q_{cond}} = \dot{m}_{ORC}(h_{14} - h_{11}) = \dot{m}_{agua}(h_{16} - h_{15})$	(22)

For the calculation of the exergy in each state within the cycle, the kinetic and potential energy changes are considered negligible, as shown in the equation, determining the physical exergy as the difference between the enthalpy potential energy and the entropy destruction.

$$ex_{phi} = \Delta h - T_0 \Delta s \tag{23}$$

where enthalpy and initial temperature are values obtained at reference conditions 101.3 kPa and 298.15 K.

Chemical exergy is defined as the work or useful energy of a chemical substance subjected to a reaction to obtain thermodynamic equilibrium. Therefore, it is considered relevant to calculate the characterization of the exhaust gases in gas turbines according to their composition and the impact they generate on the environment under the thermodynamic conditions proposed in the study system.

$$ex_{chem} = \sum_{i=1}^{n} X_i ex_{chem(i)} + RT_0 \sum_{i=1}^{n} X_i ln X_i \tag{24}$$

where X_i represents the mole fraction of the total gas and $ex_{chem(i)}$ is the mole fraction of the gases composing the total. In addition, R is the universal gas constant.

In summary, the total system exergy is the sum of the physical and chemical exergy.

$$ex_{tot} = ex_{phi} + ex_{chem} \tag{25}$$

$$\sum \dot{m}_{inlet} ex_{total\_in} - \sum \dot{m}_{output} ex_{total\_out} + \dot{Q}\left(1 - \frac{T_0}{T}\right) - W - ex_{dest} = \frac{dex}{dt} \tag{26}$$

To calculate the environmental impact of the organic working fluid, the effects of the fluid in the three phases mentioned above are considered using Equation (27), and the impact of the fluid associated with the component where the heat or work transfer is generated using Equation (28); meanwhile, to calculate the environmental impact caused by the components, Equation (29) is used:

$$I_{fluid} = I^{CON}{}_{fluid} + I^{OPM}{}_{fluid} + I^{DES}{}_{fluid} \tag{27}$$

$$I^{f}{}_{equip} = I_{fluid} \times ex^{f}{}_{equip} \tag{28}$$

$$I_{equip} = I^{CON}{}_{equip} + I^{OPM}{}_{equip} + I^{DES}{}_{equip} \tag{29}$$

Finally, the total impact produced by each component of the system is given in Equation (30):

$$I_{tot} = I_{equip} + I^{f}{}_{equip} \tag{30}$$

All parameters described in the exergo-environmental equations are given in mill points [mPts]. Multi-objective optimization problems create multiple outcomes associated with parallel values of the decision criterion parameters assigned to the study; therefore, mathematical calculations are required to identify the points closest to the ideal solution. Thus, the TOPSIS technique is used to choose the final solution based on a statistical proximity algorithm that determines the points with the shortest distance to the Positive Ideal Solution (PIS) and with the longest distance to the Negative Ideal Solution (NIS); these conditions are calculated by means of Equations (31) and (32) [28,29].

$$d_{PIS} = \sqrt{\sum_{j=1}^{n} \left(P_{ij} - P_{pj}\right)^2}, \qquad i = 1, 2, \ldots, m \tag{31}$$

$$d_{NIS} = \sqrt{\sum_{j=1}^{n} \left(P_{ij} - P_{nj}\right)^2}, \qquad i = 1, 2, \ldots, m \tag{32}$$

where i represents the iterations evaluated in each calculation up to the total number of iterations m; likewise, capital P refers to the optimal point, which is the population of the optimization.

Finally, the proximity ratio for the Ideal Solution (λ_{IS}) is obtained with Equation (33):

$$\lambda_{IS} = d_{NIS}/(d_{NIS} + d_{IS}) \tag{33}$$

where the desired value for the Ideal Solution of the problem is the value closest to 1 [30].

2.3. Selection of Biomass

The selection of biomass was based on a literature review, which considered the source of biomass, the heat capacity, the type of residue, and the amount of residue produced in the different departments of the Caribbean region.

The energy output in the heater (Stream 1) of the diagram describing the operation of the combined cycle with a hybrid energy source is equal to 756.6 kW under standard conditions as a requirement of the heat absorbed by the brine. The selection of biomass meets two relevant criteria: the resource's availability and easy accessibility. The second criterion refers to the annual biomass production in the Department of Atlántico that meets the technical specifications of commercial biomass burners.

A commercial biomass burner provides a thermal power of 300 to 1500 kW through a consumption range between 30 and 300 kg of biomass per hour of operation; therefore, to meet the demand of the combined cycle, it must be guaranteed that the biomass used provides at least 300 kg/h. Based on Table 2, the type of biomass that guarantees this minimum consumption rate is cassava peel with 53,896 tons per year; considering a resource capture of 10% (acquisition in the market, collection, derived by-product), the amount that can be supplied to the combined cycle is 615.2 kg/h.

Table 2. Energy potentials of different biomasses in the Caribbean region of Colombia [31].

Departments	Source	Production (t/year)	Waste	PCI (kcal/kg)
Atlántico	Cassava	53,896	Cassava peel	2.151
	Corn	15,035	Stubble	3.429
			Tusa	3.39
			Capacho	3.815
			Dry leaves	4.274
Bolívar	Rice	62,471	Chaff	3.113
			Husk	3.603
	Corn	82,343	Stubble	3.429
			Tusa	3.39
			Capacho	3.815
			Dry leaves	4.274
	Cassava	321,974	Cassava peel	2.151

Table 2. *Cont.*

Departments	Source	Production (t/year)	Waste	PCI (kcal/kg)
Cesar	Oil palm	194,184	Kernel	3.988
			Fiber	4.274
			Rachis	4.021
	Rice	86,850	Chaff	3.113
			Husk	3.603
Córdoba	Rice	135,405	Chaff	3.113
			Husk	3.603
	Corn	143,816	Stubble	3.429
			Tusa	3.39
			Capacho	3.815
			Dry leaves	4.274
	Banana	664,200	Rachis	1.809
			Stem	2.032
Guajira	Corn	36,244.32	Stubble	3.429
			Tusa	3.39
			Capacho	3.815
			Dry leaves	4.274
	Banana	46,525	Rachis	1.809
			Stem	2.032
			Refusal	2.488
	Oil palm	5925	Kernel	3.988
			Fiber	4.274
			Rachis	4.021
Magdalena	Banana	413,790	Rachis	1.809
			Stem	2.032
			Refusal	2.488
	Oil palm	104,104	Kernel	3.988
			Fiber	4.274
			Rachis	4.021
Sucre	Rice	152,495	Chaff	3.113
			Husk	3.603
	Corn	16,052	Stubble	3.429
			Tusa	3.39
			Capacho	3.815
			Dry leaves	4.274
	Oil palm	16,085	Kernel	3.988
			Fiber	4.274
			Rachis	4.021

2.4. Working Fluid Selection

The algorithm designed for calculating the cycle conditions under study has a simulation linked to the NIST REFPROP software v9.1, where more than 120 pure and mixed fluids are found for modeling systems with organic cycles. Initially, the main commercial and readily available organic fluids are identified for the identification and evaluation of thermo-physical properties by means of an investigation limited to fluids applied in power generation systems. The main options are listed in Table 3:

Table 3. Properties of commercial organic fluids.

Ref.	Organic Fluid	Pc	Tc	GWP	ODP	Type
[32]	Cyclohexane	4075	553.6	Low	0	Dry
[32]	Benzene	4894	562.1	Low	0	Isentropic
[32]	R245fa	3651	427.0	950	0	Dry
[33]	R134a	4059	374.2	1370	0	Wet
[33]	Toluene	4109	591.8	-	-	Dry
[34]	Acetone	4600	507.9	-	-	Isentropic
[34]	Ethanol	6268	514.6	-	-	Wet
[34]	R11	4407	471.1	4600	1	Isentropic

The criteria for selecting the fluids were established to align with both thermodynamic and environmental performance goals:

Environmental criteria: Fluids with zero or low global warming potential (GWP) and ozone depletion potential (ODP) were prioritized to meet sustainability objectives and environmental regulations under ASHRAE 34-2001 and NFPA 704 within classifications A1, B1, A2L, B2L, and some criteria are taken into account, such as thermal stability, flammability, and toxicity [35].

Thermodynamic properties: The fluids were selected based on critical pressure (Pc) and temperature (Tc) because these parameters directly influence the low-temperature waste heat recovery, net power of the ORC cycle, equipment acquisition cost, and, hence, the overall thermal efficiency of the system.

Three working fluids were shortlisted based on these criteria: cyclohexane, acetone, and toluene. All three are useful for waste heat recovery applications. Both cyclohexane and toluene are "dry" fluids, making them ideal for applications where waste heat temperatures are greater than 200 °C, typical of industrial sources such as furnaces or chemical processes. On the other hand, acetone, with "isentropic" properties, is suitable for moderate temperature ranges, between 150 °C and 200 °C, found in lower process waste heat recovery systems, such as thermal effluents. These fluids not only meet environmental requirements but also, by their nature, fit low-temperature profiles in low-temperature waste heat utilization [36].

Finally, sensitivity results will be obtained with the selected fluids in terms of net power, pinch point, efficiency, and destroyed exergy to choose the ideal working fluid.

2.5. Model Validation

To validate the thermodynamic model, the operating conditions of the proposed system were selected from a previous literature review. In addition, it was decided to validate each system independently, since accurate data from other studies are not available. In this context, Table 4 presents the input parameters for the Brayton and ORC cycles, considering R245fa as the working fluid in the latter. Figure 2 shows the behavior of the thermal efficiency of the Brayton cycle as a function of the turbine inlet temperature. In

contrast, Figure 3 illustrates the variation in the thermal efficiency of the ORC with respect to the heat source temperature.

Table 4. Model validation input variables.

Ref.	Proposed Systems	Input Parameters	Value
[37]	Brayton sCO_2	Direct normal irradiance	980 W/m^2
		Ambient temperature	35.5 °C
		Turbine efficiency	93%
		Compressor efficiency	89%
		Heat exchanger effectiveness	95%
		Turbine inlet temperature	500–800 °C
		Cycle high pressure	25 MPa
		Minimum pinch point temperature	5 °C
		Initial temperature difference	20 °C
		Reference temperature	25 °C
		Reference pressure	101.325 kPa
[38]	ORC	Thermal source temperature	100–200 °C
		Minimum difference of approximation	10, 20, 30, Saturation
		Pinch temperature difference	10 °C
		Condensation temperature	40 °C
		Turbine isentropic efficiency	85%
		Pump isentropic efficiency	85%
		Working fluid	R245a

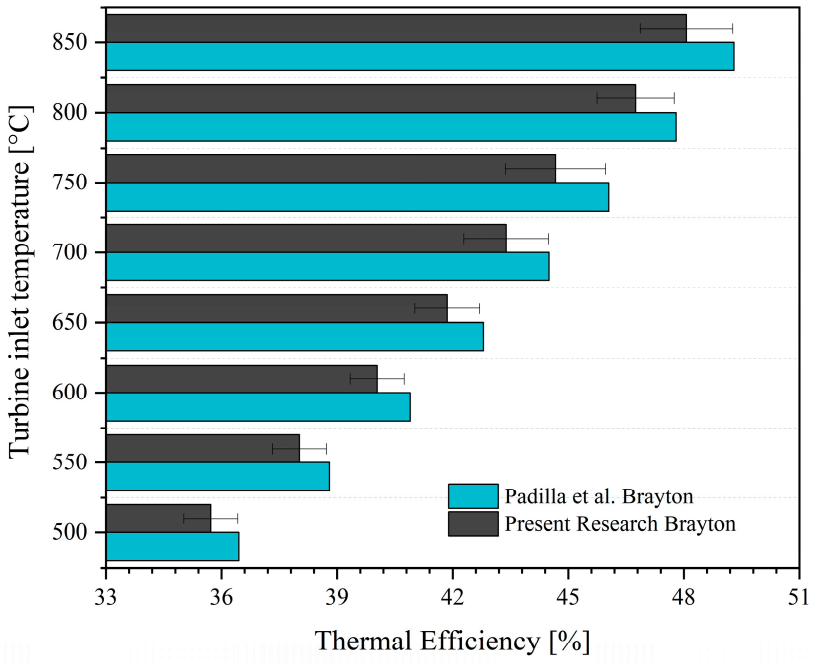

Figure 2. Model validation: Brayton supercritical sCO_2 [37].

Figure 2 compares the results obtained by Padilla et al. [37] with those of the model proposed in this study, showing that, in both cases, an increase in the turbine inlet temperature generates a slight increase in thermal efficiency. A consistent trend is observed in the alignment of the values, with a maximum margin of error of 3%. These differences could be related to the assumed reference conditions or the model's fluids.

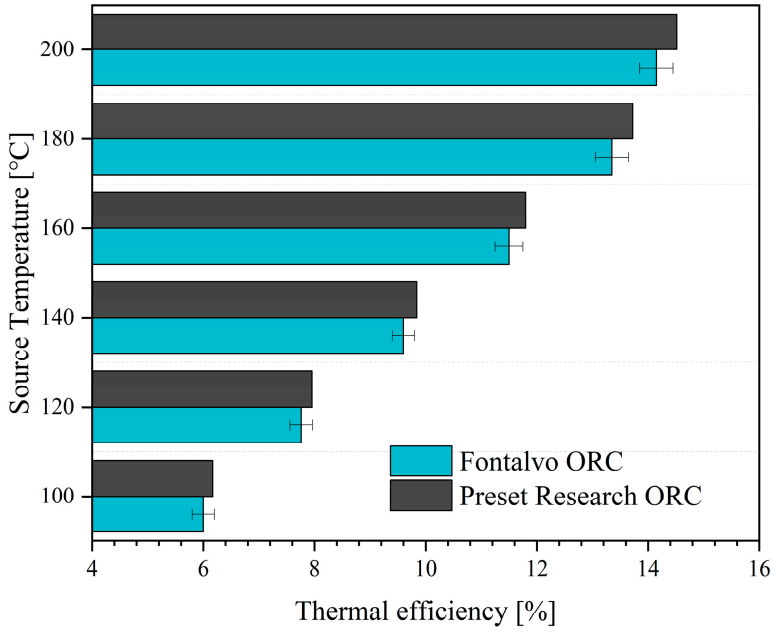

Figure 3. Model validation: organic Rankine cycle.

On the other hand, in Figure 3, for values above 130 °C, the behavior of the proposed model closely matches the model presented by Fontalvo et al. [38], showing relative discrepancies of up to 3%. This supports the accuracy and validity of the results obtained in this study.

3. Results and Discussion

The performance evaluation was developed with a thermodynamic analysis based on the energetic, exergetic, and environmental performance of the parameters that describe the fundamental structure of the hybrid system for electric power generation.

The operating conditions for the Brayton/ORC combined cycle with integrated recompression for waste heat recovery have solar radiation of 950 W/m^2 K, the initial heat recovery efficiency (EHR) is 0.85, the turbine inlet temperature is 1008.15 K, the high pressure for the system is 25,000 kPa, the isentropic efficiency of the turbines is 0.8, the pressure ratio is 10, the pinch point of the evaporator is 10, the isentropic efficiency for the compressor is 0.8, as well as for the turbine, and, finally, the ambient operating temperature is 328 K.

3.1. Environmental Analysis

The environmental impacts are calculated using Equations (27)–(30). Under the initial operating conditions, the ratio of exergy destroyed by components and the traditional environmental exergy impacts are considered for the system under study.

Where power and heat are in kW, w_mat is the material factor in mPts/kg, and environmental impact variables are in mPts. As shown in Table 5, the solar tower generates the most significant amount of total environmental exergy impact, with a percentage of 44.29% compared to the total. In the case of the burner, turbine (T3), heater, and condenser, it was observed that they are responsible for 27.06%, 8.85%, 1.63%, and 1.04% of the total environmental exergy impact. The participation of the rest of the components in the total environmental exergy impact is less than 1%. The high environmental energy impact in the burner may be a consequence of combustion irreversibilities, which may be associated with temperature gradients and chemical reactions. On the other hand, the burner has thermal

losses to the environment, and non-utilized heat is generated. Similar results are reported in the literature [39].

Table 5. Environmental impacts and LCA for steel and cyclohexane.

Component	$\dot{W}$	$\dot{Q}$	w_mat	ex^{f}_{equip}	I_{fluid}	I^{CON}_{equip}	I^{OPM}_{equip}	I^{DES}_{equip}	I_{tot}
C1	38.27		86	0.010	12.46	126.562	0	39.85	166.53
C2	18.68		86	0.019	31.06	256.12	0	32.64	289.35
T1	66.58		86	0.006	8.5	1156.33	0	102.56	1258.94
T2	116.17		86	0.010	4.6	1154.29	0	89.23	1243.56
HR		176.42	86	0.060	69.23	22,145.6	0	256.85	22,406.60
HTR		477.04	86	0.068	56.24	2365.79	0	456.21	2825.82
RHR		68.03	86	0.047	56.8	4562.81	0	389.14	4954.61
LTR		167.07	86	0.008	49.74	1244.5	0	368.6	1613.49
Cooler		55.91	86	0.024	26.38	3684.13	0	1136.3	4821.06
Evaporator		74.96	86	0.004	104.56	4102.36	0	4536.36	8639.13
T3	8.23		86	0.000	9.3	985.36	0	120,874	121,859.56
P2	0.01		86	0.000	1.9	468.23	0	46.25	514.48
Condenser		64.02	86	0.012	47.12	14,261	0	12.13	14,261.58
Burner		73.04	86	0.493	4.61	123,658	248,759	10.38	372,430.10
Solar tower		407.31	86	0.239	1.23	263,785	345,871	12.45	609,669.20
Organic fluid					483.73	84,562	98,456	26,587	209,605.17
Total	247.93	1563				528,520	693,086	154,938	1,376,559.26

The operating conditions of the system are shown in Table 6. These data were used as input data for the mathematical model implemented in MATLAB. From the results obtained, an initial analysis was performed. After this, a sensitivity study was performed using three organic working fluids and CO_2 as SBC fluid.

Table 6. Initial conditions in the system with superheat.

Parameter	Unit	Initial Value
T_1	K	1073.15
P_3	kPa	25,000
η_t	%	90
η_c	%	90
AP	°C	39
r_p	-	15
$T_{Pinch\text{-}cond}$	K	10
$T_{pinch\text{-}Evap}$	K	7.71
T_{cond}	K	313.15
e_{HTR}	%	95
e_{LTR}	%	95
T_6	K	328.15

Tables 7 and 8 show the system performance parameters obtained from the thermodynamic properties of both configurations. The net power of the Brayton cycle with a reheat is shown in the first column, followed by the total heat generated in the combined cycle heat exchangers, the energy contribution provided by the heat source (biomass), and the energy contribution of the solar collection system; finally, it shows the first- and second-law efficiencies.

Table 7. Energy and exergy performance at initial conditions with superheat.

$\dot{W}_{net}$	Q_{tot}	E_{bio}	E_{solar}	E_{tot}	η_I	η_{II}
155.8	311.31	87.52	530.50	618	45.80	25.22

Table 8. Energy and exergy performance at initial conditions with superheat and recompression.

$\dot{W}_{net}$	Q_{tot}	E_{bio}	E_{solar}	E_{tot}	η_I	η_{II}
134	311.31	87.52	530.50	618	54.85	27.92

where all energies and net power are in kW. For the exergy evaluation, the determination of the different types of exergies is shown in Table 9.

Table 9. Exergetic analysis by component.

Components	ex_{input}	ex_{prod}	ex_{loss}	ex_{dest}
C1	58.14	54.02	-	4.12
C2	49.19	41.05	-	8.14
T1	82.40	79.77	-	2.63
T2	125.37	121.23	-	4.14
HR			-	0.00
HTR	346.13	320.28	-	25.85
RHR	87.50	58.15	-	29.35
LTR	241.50	221.30	-	20.20
Cooler	229.60	222.36	3.59	3.65
Evaporator	31.27	21.14	-	10.13
T3	14.85	13.01	-	1.85
P2	0.02	0.01	-	0.002
Condenser	6.41	0.11	1.01	5.29
Solar tower	-	-	-	212.23
	-	-	55.44	102.95
Total	981.69	890.08	60.04	402.18

From the results shown above, we see that the largest amount of exergy destroyed occurs in the equipment where the phenomenon of heat energy transfer occurs; this is in the heater (HTR) and presents 6.43% of total system losses. In the Re-Heater (R-HTR), there is 7.30% of the exergy destruction, and, finally, in the evaporator, there is 2.52% destruction. A great deal of research has been developed to find ways to mitigate the exergy losses in these components; one of the most promising is the use of entropic mixtures as working fluid (where applicable) given the great effectiveness they have shown in reducing irreversibilities. The solar tower is the main source of exergy destroyed by the hybrid system with a value of 212.23 kW, which represents 52.77% of the total exergy destroyed. The high exergy destruction in the solar tower is a consequence of the solar tower field. This may be a consequence of various factors, such as inefficiency in the solar radiation capture process, convective and radiative heat losses, or thermal irreversibilities due to the high temperature difference between the working fluids. Similar results have been reported in the literature [40].

3.2. Sensitivity Analysis

This section aims to evaluate the effect of operational parameters on the performance of the combined cycle in two configurations (SBC-ORC Superheat and SBC-ORC Superheat and recompression). The purpose is to perform a sensitivity analysis, which allows for the identification of the input parameters that significantly affect the performance of

the combined cycle. The variables used to analyze the performance of the cycle are net power generation, total destroyed exergy, and exergy–waste ratio (EWR). The operational parameters selected are turbine inlet temperature, turbine efficiency, compressor efficiency, evaporator pinch point (AP), pressure ratio (r_p), and high pressure.

3.2.1. Sensitivity Analysis (SBC-ORC Superheat)

Figure 4 shows the effect of operational parameters on the net power generation of the combined cycle with three working fluids (toluene, acetone, and cyclohexane).

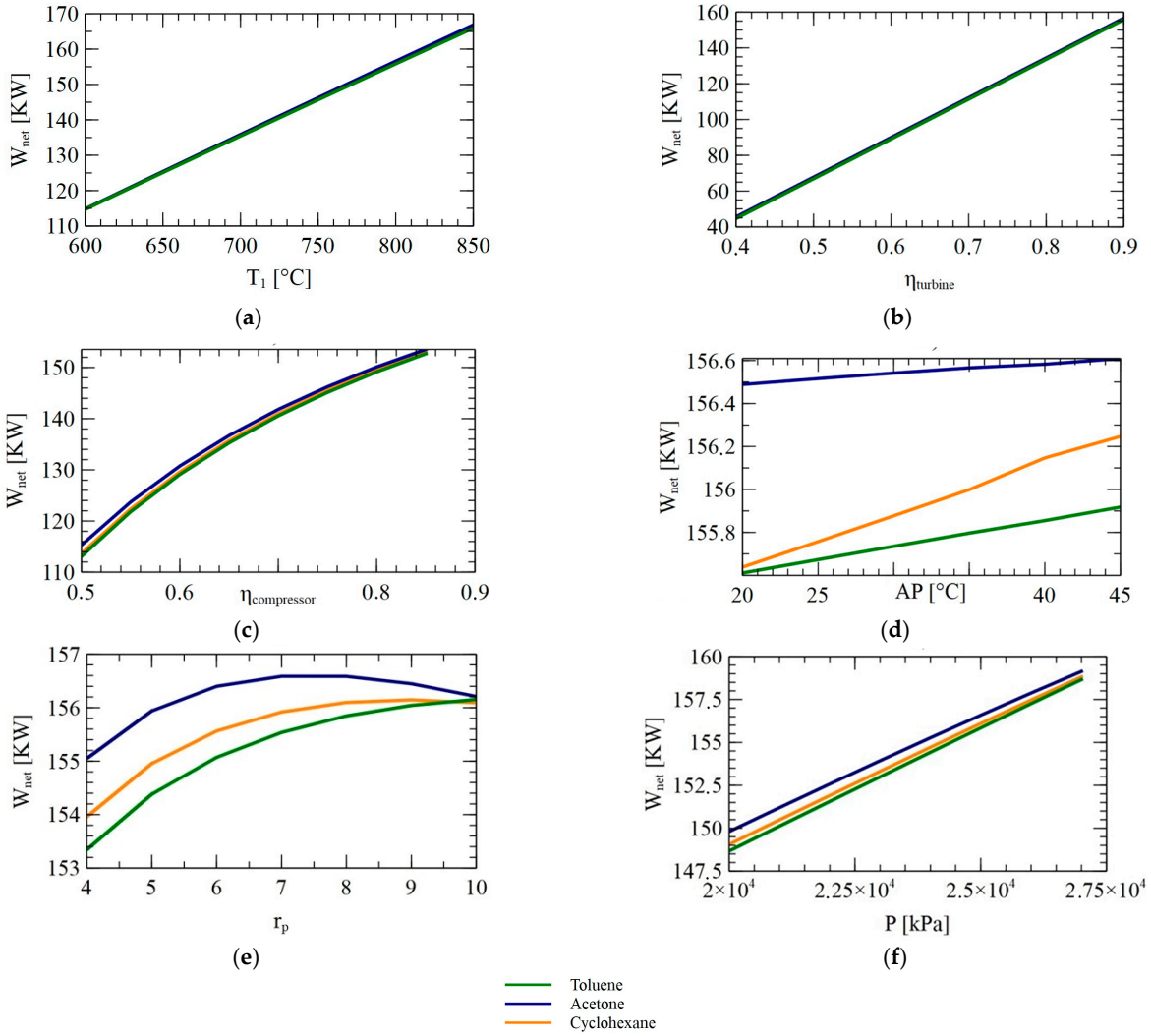

Figure 4. Change in net power generation (W_{net}) with different fluids under variations in performance parameters in SBC-ORC Superheat: (**a**) T_1, (**b**) $\eta_{turbine}$, (**c**) $\eta_{compressor}$, (**d**) AP, (**e**) r_p, and (**f**) pressure.

Figure 4a–c show that the type of working fluid does not significantly affect the net power generation when the turbine inlet temperature, turbine efficiency, and compressor efficiency are varied. The increase in the above operational parameters causes an increase in the net power generation following a linear behavior, independently of the type of working fluid. When variations are made in the evaporator pinch point, pressure ratio, and high pressure, acetone achieves a higher net power generation, followed by cyclohexane and toluene, as shown in Figure 4d–f. On the other hand, it is observed that the increase in the operational parameters of the evaporator pinch point and high pressure leads to higher levels of net power generation. However, Figure 4e shows that pressure ratio (r_p) values

higher than 7.5 lead to a reduction in the net power generation in the combined cycle, except for in the case of toluene.

Figure 5 shows the effect of operational parameters on the total destroyed exergy in the combined cycle with three various working fluids (toluene, acetone, and cyclohexane).

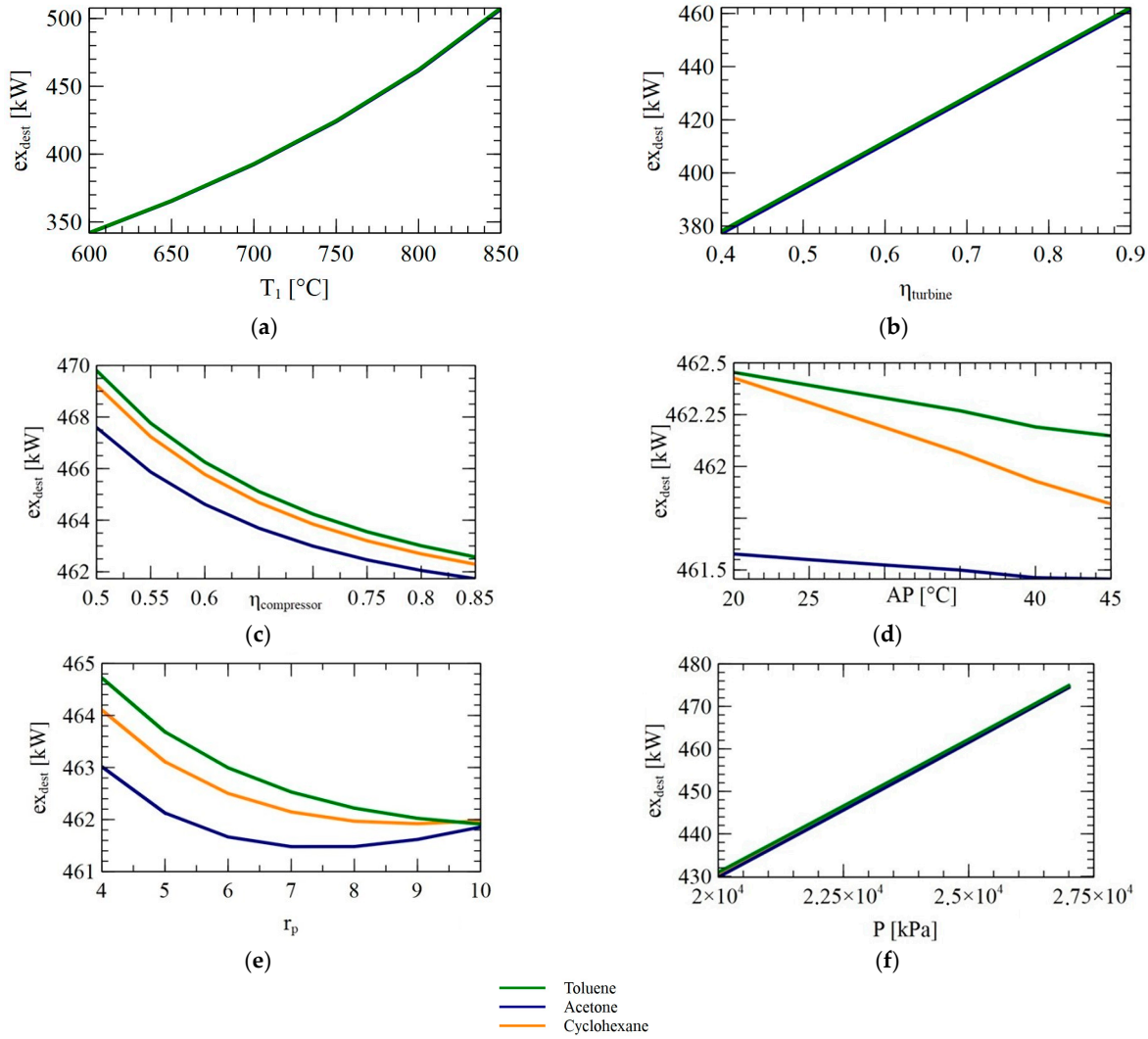

Figure 5. Change in the total destroyed exergy (ex_{dest}) with different fluids under variations in performance parameters in SBC-ORC Superheat: (**a**) T_1, (**b**) $\eta_{turbine}$, (**c**) $\eta_{compressor}$, (**d**) AP, (**e**) r_p, and (**f**) pressure.

In the case of Figure 5a,b,f, a higher total destroyed exergy is shown as the turbine inlet temperature, turbine efficiency, and high-pressure increase, independently of the working fluid. This increase in total destroyed exergy follows an approximately linear correlation as a function of the mentioned operational parameters. In Figure 5c,d,e, it is observed that the increase in compressor efficiency, evaporator pinch point, and pressure ratio tend to reduce the total destroyed exergy by the combined cycle. However, a correlation that describes the behavior shown in the figures cannot be clearly evidenced. On the other hand, it can be demonstrated that acetone achieves the lowest total destroyed exergy for the operating ranges analyzed compared to cyclohexane and toluene.

Figure 6 shows the effect of operational parameters on the exergy–waste ratio (EWR) in the combined cycle with three various working fluids (toluene, acetone, and cyclohexane).

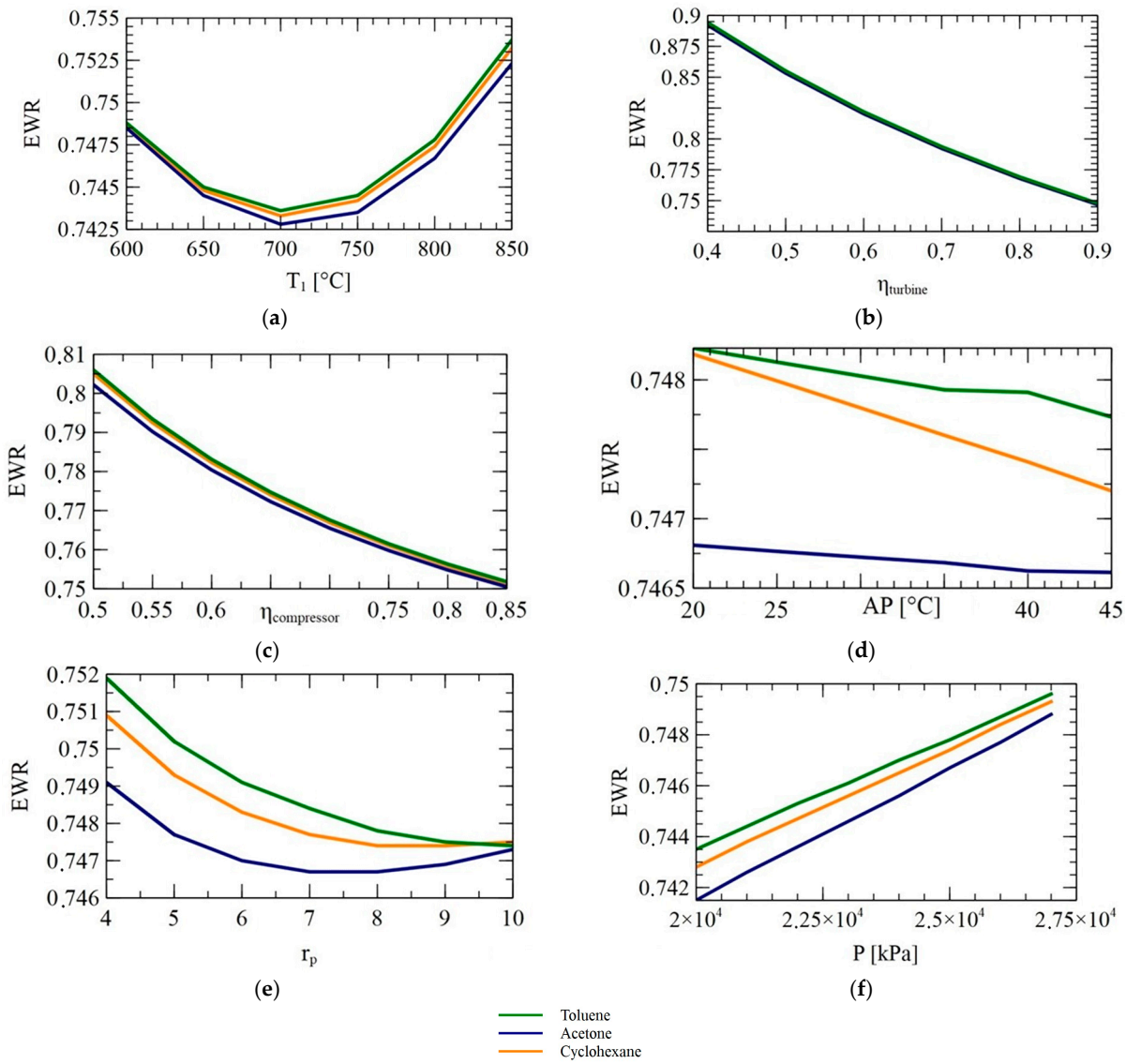

Figure 6. Change in EWR with different fluids under variations in performance parameters in SBC-ORC Superheat: (**a**) T_1, (**b**) $\eta_{turbine}$, (**c**) $\eta_{compressor}$, (**d**) AP, (**e**) r_p, and (**f**) pressure.

The analysis in Figure 6 shows that acetone reduces the exergy–waste ratio for each of the selected operational parameters, followed by cyclohexane and toluene. This reduction becomes more noticeable with the variation in operational parameters such as evaporator pinch point, pressure ratio, and high pressure. The exergy–waste ratio presents various behaviors depending on the operational parameter. Increasing turbine efficiency, compressor efficiency, and evaporator pinch point generally tends to reduce the exergy-waste ratio. However, it was observed that values above 700 °C in the turbine inlet temperature cause an increase in the exergy–waste ratio. Similarly, trends indicate that values higher than 7.5 in pressure ratio lead to higher levels of the exergy–waste ratio.

3.2.2. Sensitivity Analysis (SBC-ORC Superheat and Recompression)

Figure 7 shows the effect of operational parameters on the net power generation of the combined cycle with three various working fluids (toluene, acetone, and cyclohexane).

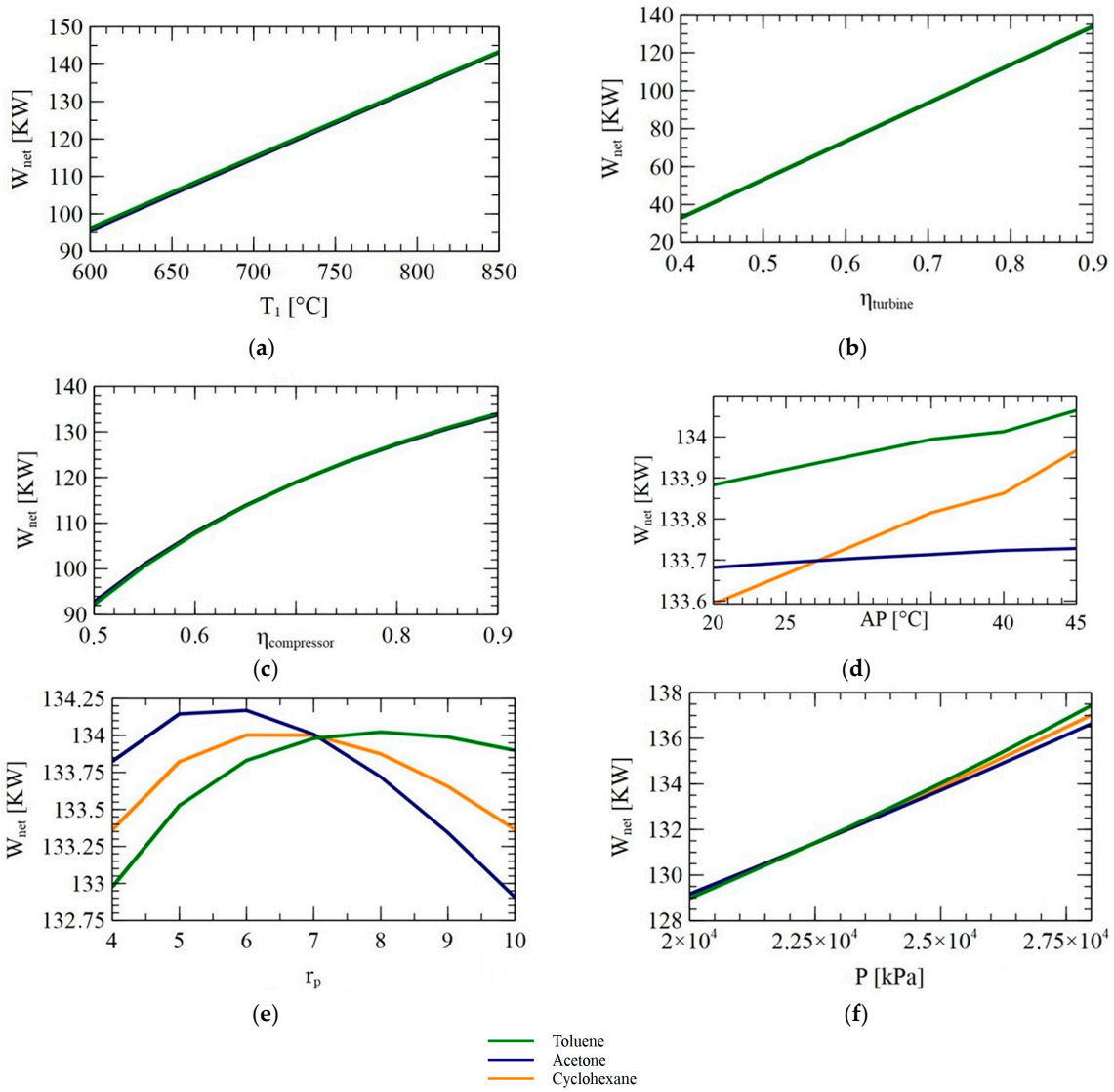

Figure 7. Change in power generation (W_{net}) with different fluids under variations in performance parameters in SBC-ORC Superheat and recompression, (**a**) T_1, (**b**) $\eta_{turbine}$, (**c**) $\eta_{compressor}$, (**d**) AP, (**e**) r_p, and (**f**) pressure.

The results in Figure 7 show that the increase in turbine inlet temperature, turbine efficiency, compressor efficiency, and high pressure must increase the net power generation in the combined cycle. As in the previous system, this behavior is independent of the working fluid used and is in agreement with the results obtained by Tovar et al. [36], who performed a very similar energy study integrating a supercritical Brayton cycle with reheat and recompression with a dual-loop ORC. The few differences in power generation by the systems using different working fluids are due to the fact that the main Brayton system provides the largest amount of power production making the contribution of the ORC systems very small (~3–4%) and the differences observed graphically are little.

In the case of evaporator pinch point and pressure ratio, various trends are observed depending on the operational parameter value and the working fluid type. Figure 5d shows that toluene achieves a higher net power generation for the evaporator pinch point variation range. For values above 27.5 °C at the evaporator pinch point, it is observed that cyclohexane achieves higher net power generation than acetone. Toluene also achieves the highest net power generation for pressure ratio values above 7.

Figure 8 shows the effect of operational parameters on the total destroyed exergy in the combined cycle with three various working fluids (toluene, acetone, and cyclohexane).

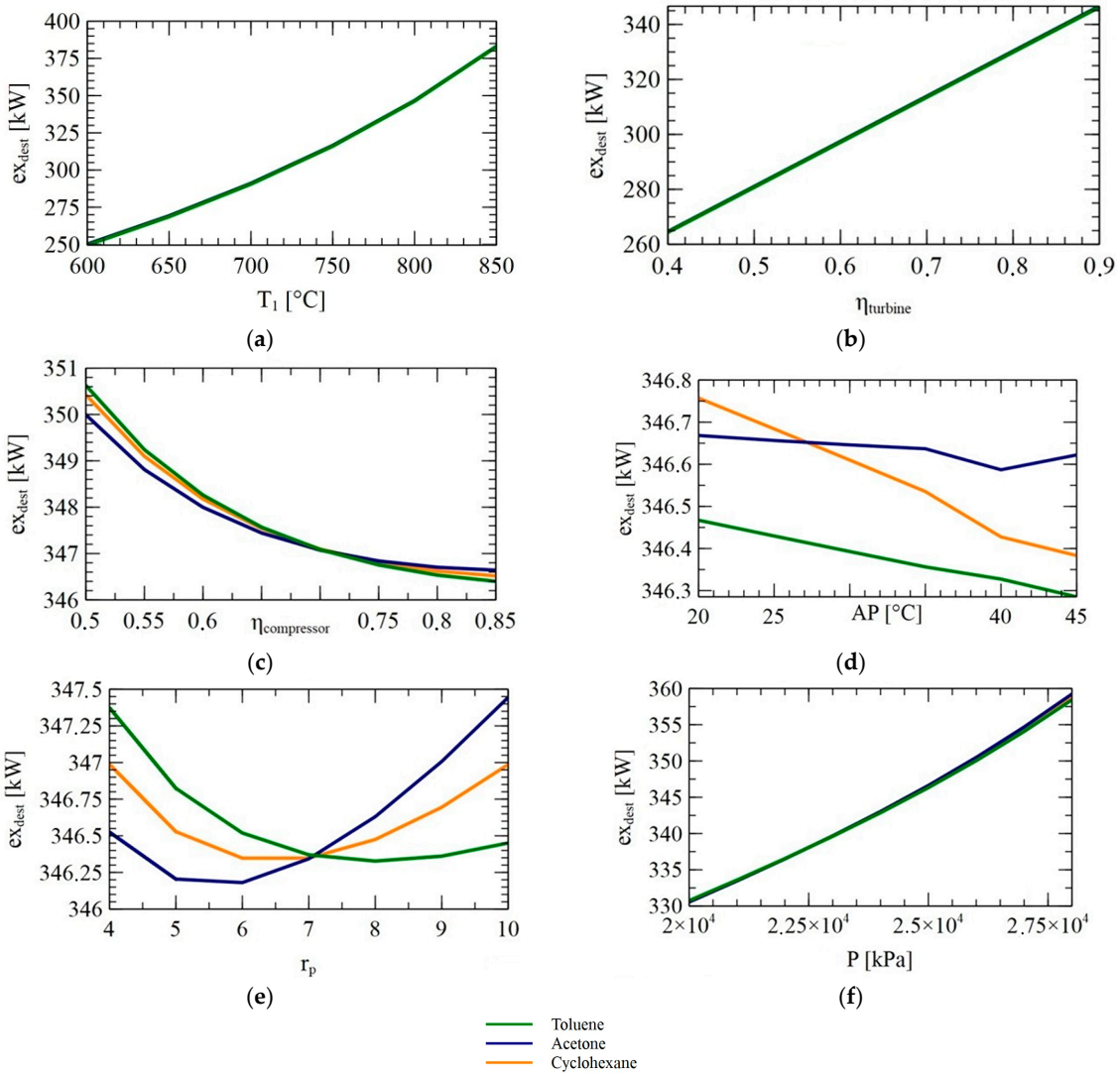

Figure 8. Change in the destroyed exergy (ex_{dest}) with different fluids under variations in performance parameters in SBC-ORC Superheat and recompression: (**a**) T_1, (**b**) $\eta_{turbine}$, (**c**) $\eta_{compressor}$, (**d**) AP, (**e**) r_p, and (**f**) pressure.

The trends in Figure 8a,b,f show that the total destroyed exergy tends to increase with the values of turbine inlet temperature, turbine efficiency, and high pressure. This behavior was observed for all three working fluids. In general, toluene is the working fluid that achieves the lowest destroyed exergy. However, the cycle must operate with a compressor efficiency greater than 0.70 and a pressure ratio greater than 7.

Figure 9 shows the effect of operational parameters on the exergy–waste ratio (EWR) in the combined cycle with three various working fluids (toluene, acetone, and cyclohexane).

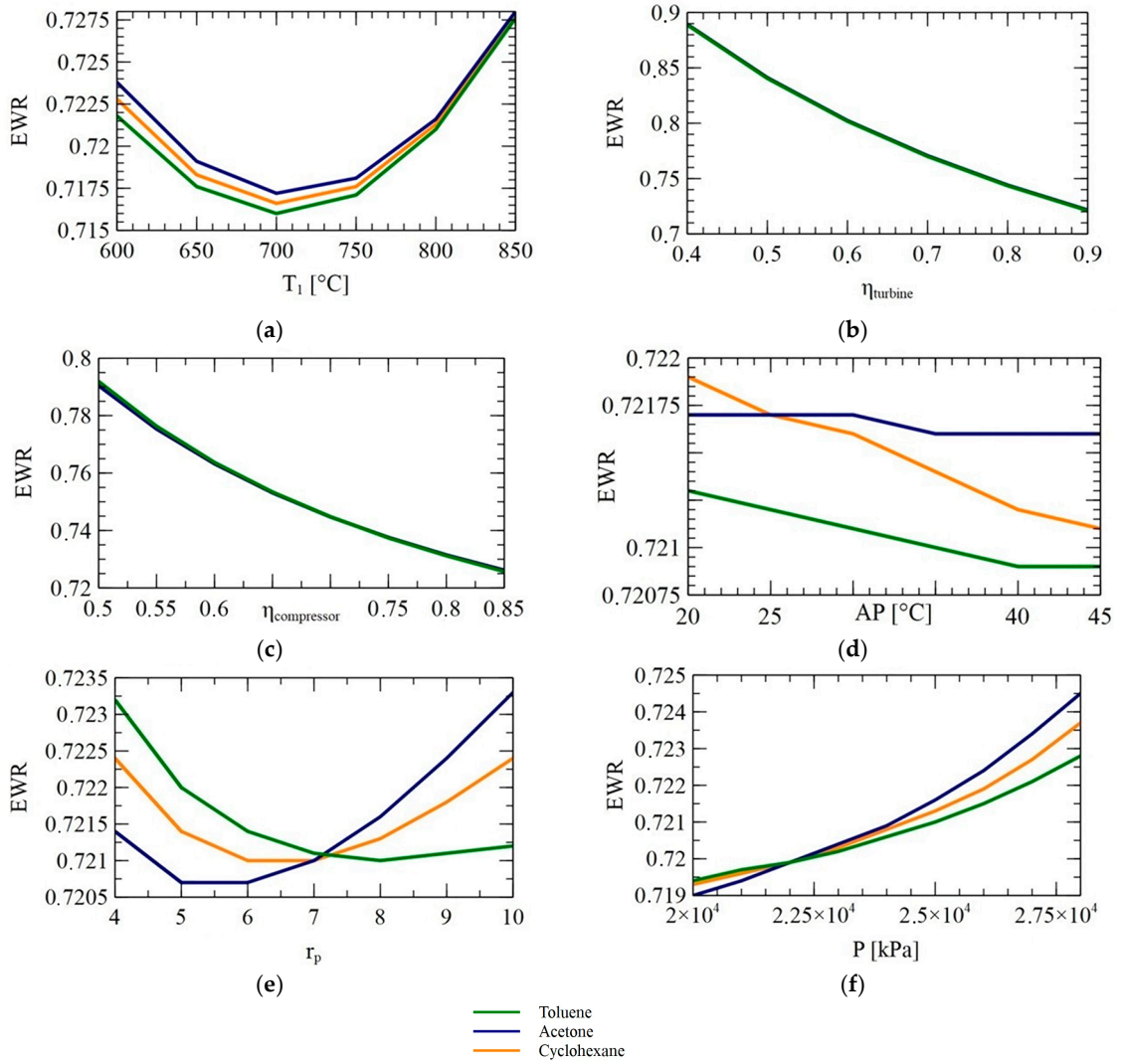

Figure 9. Change in EWR with different fluids under variations in performance parameters in SBC-ORC Superheat and recompression: (**a**) T_1, (**b**) $\eta_{turbine}$, (**c**) $\eta_{compressor}$, (**d**) AP, (**e**) r_p, and (**f**) pressure.

The results in Figure 9b,c show that the increase in turbine efficiency and compressor efficiency reduces the exergy–waste ratio of the combined cycle independently of the working fluid. Among the three working fluids analyzed, toluene has a greater ability to reduce the exergy–waste ratio. However, this requires the combined cycle to operate with pressure ratio values greater than 7 and a high pressure greater than 2.25×10^4 kPa. On the other hand, it was observed that acetone is the working fluid that tends to cause higher levels of the exergy–waste ratio.

3.3. Correlation Analysis

A correlation matrix was used to identify the most significant variables that influence the target variable to ensure high precision in the optimization model. The correlation coefficient values vary from −1 to +1, where +1 indicates a linear proportional relationship, which implies that as one variable increases, the other also increases. Meanwhile, a coefficient value of −1 signifies an inversely proportional relationship, where one variable increases as the other decreases. On the other hand, a coefficient value of zero indicates that there is no linear correlation between the variables.

Figure 10 shows the correlation matrices of the operational parameters and the combined cycle output variables for two configurations: SBC-ORC Superheat and SBC-ORC Superheat and recompression.

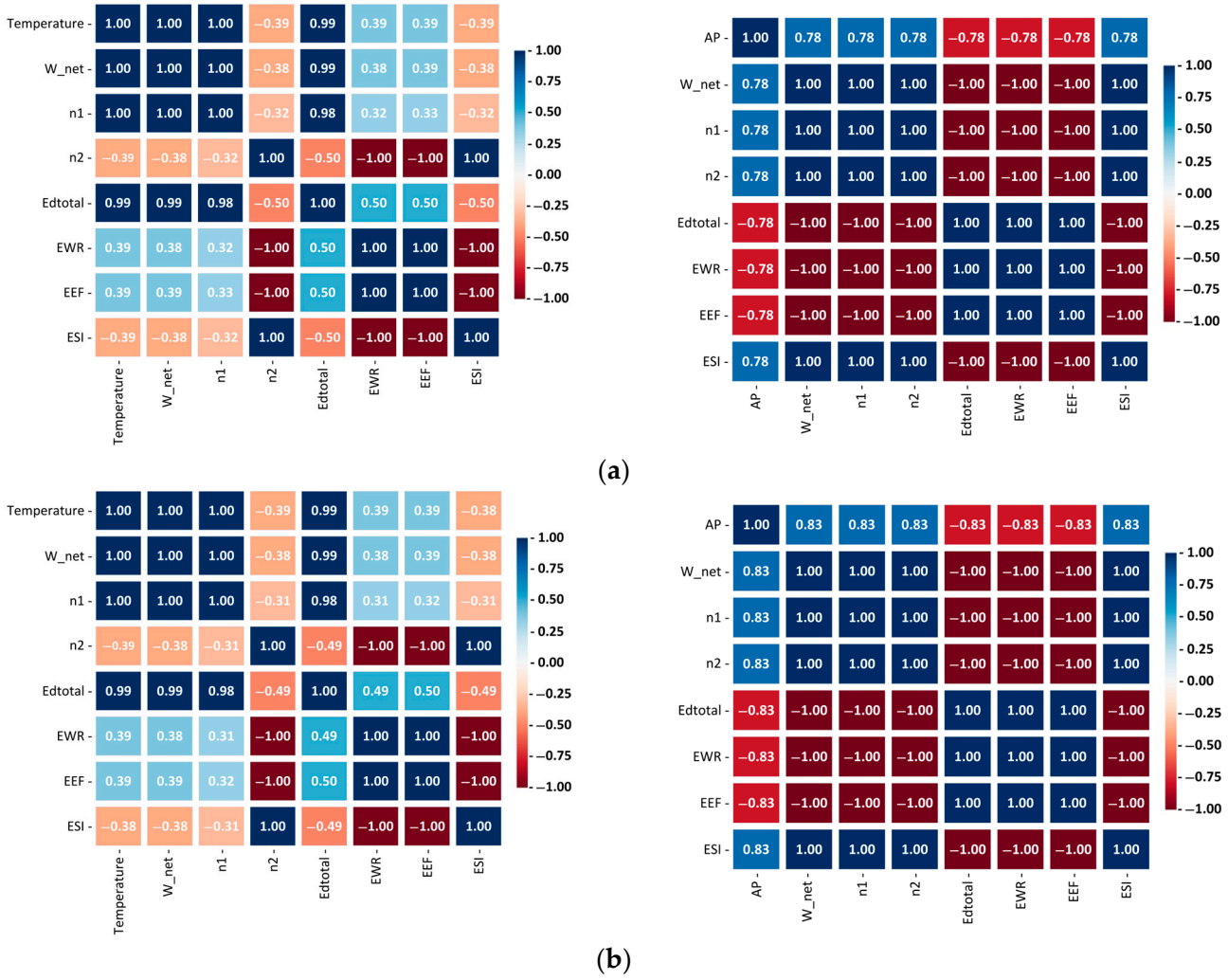

Figure 10. Correlation matrix of the combined cycle: (**a**) SBC-ORC Superheat and (**b**) SBC-ORC Superheat and recompression.

The heat map shows which variables have strong correlations with each other. For example, Figure 10a shows that inlet turbine temperature has a high positive correlation (≥ 0.99) with important performance variables in the combined cycle, such as net power generation (W_net) and total destroyed exergy (Edtotal). In the case of Figure 10b, it is observed that the evaporator pinch point (AP) also presents a high positive correlation (≥ 0.78) with performance variables such as net power generation and the exergetic sustainability index (ESI). Additionally, the evaporator pinch point has a high negative correlation with variables such as total exergy destroyed (Edtotal), exergy–waste ratio (EWR), and environmental effect factor (EEF). This shows that the inlet turbine temperature and the evaporator pinch point are performance parameters that significantly affect the performance of the combined cycle (SBC-ORC Superheat). From the results of Figure 10b, it can also be observed that the variables inlet turbine temperature and evaporator pinch point have a significant positive and negative correlation with the performance variables of the combined cycle (SBC-ORC Superheat and recompression).

3.4. Multi-Objective Optimization

The selection of the decision criteria for the optimization is based on the result of the correlation analyses for both configurations from the parameters that significantly influence (positive and negative) the environmental exergy indicators calculated during the section. For this study, the input parameters for the algorithm that impact the exergy indicators are the pinch point of the evaporator and the inlet temperature at T1 that receives the waste energy from the solar–biomass hybrid source. The optimization was performed with a generic algorithm for a population of 200 values and 102 interactions for each evaluated configuration. To guarantee the interaction of the four decision variables, the optimized function is specified with a double vector and conditioned by the restrictions of the variables, as described in Table 10.

Table 10. Decision criteria for multi-objective optimization.

Variable	Symbol	Minimum Value	Maximum Value	Criteria
Inlet turbine temperature 1 [°C]	T_1	600	850	C1
Evaporator pinch point [°C]	AP	20	45	C2
Pressure ratio	r_p	2	12	C3
Destroyed exergy [kW]	ex_{dest}	340	510	C4

For the optimization curve to be relevant in the description and discussion of the optimization results, it is necessary to know the behavior of the criteria during the iteration process to minimize the objective functions and, therefore, the relevance of one or another variable concerning the result obtained. For this reason, the distribution profile is obtained for the data population in the multivariate analysis. Figures 11 and 12 shows the operating ranges in which the decision variables were evaluated for the two combined cycle configurations.

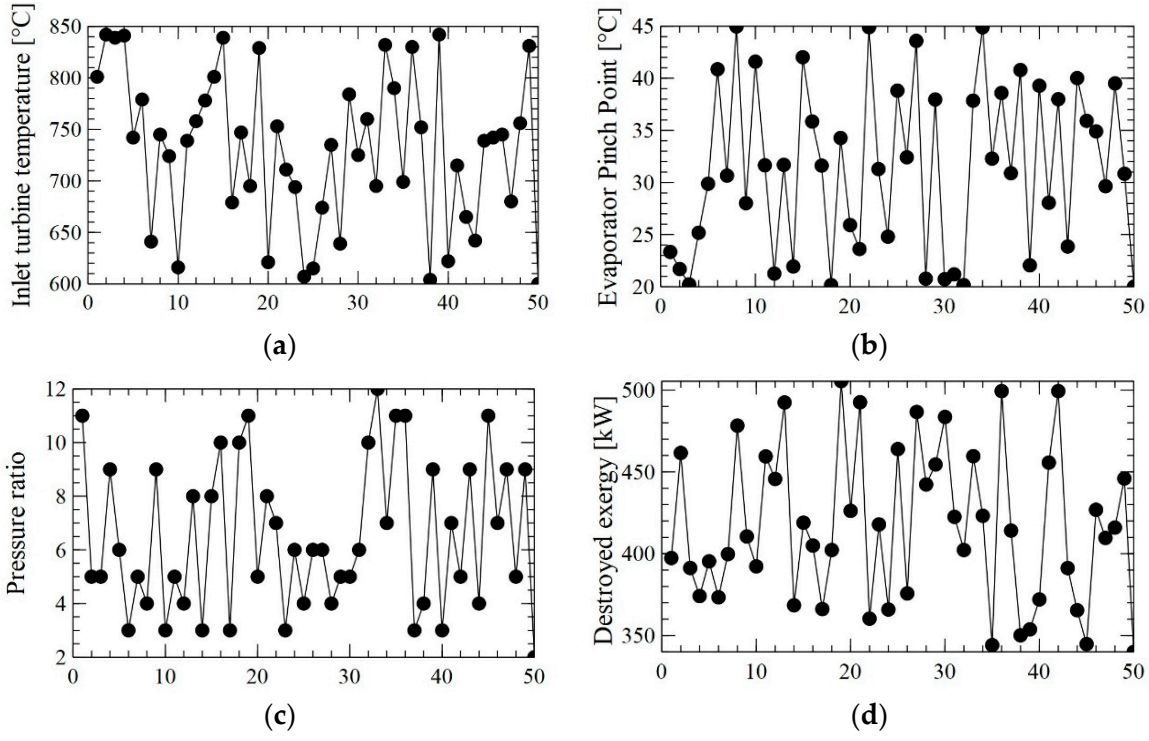

Figure 11. Sparse distribution of the Pareto frontier population in the configuration with superheat; (**a**) T_1, (**b**) AP, (**c**) r_p, and (**d**) $ex_{dest.}$.

The operating limits for the inlet turbine temperature parameter for both configurations were 600–850 °C, as shown in Figures 11a and 12a. These figures show that the best operating conditions occur at high temperatures (higher concentration of data clouds). For the evaporator pinch point and pressure ratio parameters, more significant variability in the data cloud was observed for the established limits.

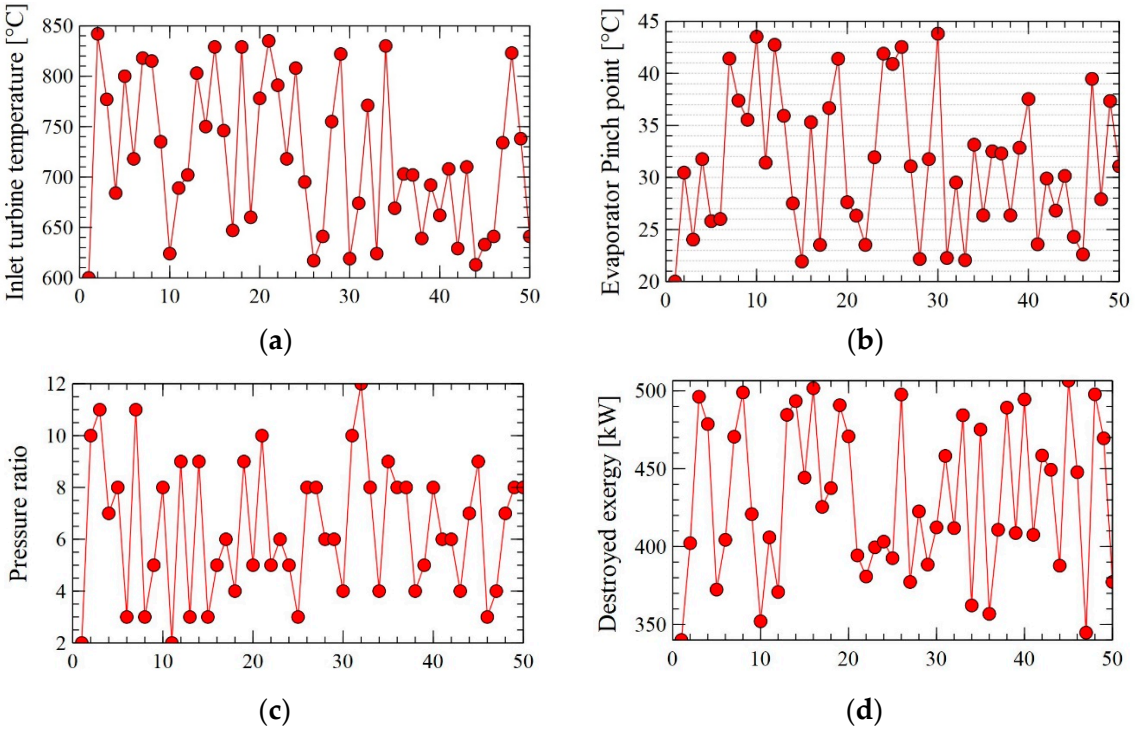

Figure 12. Sparse distribution of the Pareto frontier population in the configuration with superheat and recompression; (**a**) T_1, (**b**) AP, (**c**) r_p, and (**d**) $ex_{dest.}$.

The behavior infers a correct correlation of each of the criteria through the formulation of the equations during the creation of the algorithm, obtained through the nonlinear regression of the objective functions. Thus, the functions are determined based on the selected criteria:

$$\text{minEWR} = a_1 \times T_1 + a_2 \times T_1 \times r_p + a_3 \times AP^2 + a_4 \times r_p + a_5 \times ex_{dest} + k \quad (34)$$

$$\text{minEEF} = b_1 \times T_1 + b_2 \times AP \times r_p + b_3 \times AP + b_4 \times r_p + b_5 \times {ex_{dest}}^2 + k \quad (35)$$

where the coefficients k, a_n, and b_n are calculated using a nonlinear regression algorithm in MATLAB by obtaining the results of the thermodynamic parameters in response to the variation in the input variables in the overall system (Table 11).

Figure 13 shows the distribution of the optimal values for the different study configurations between the zones of Ideal Solutions (ISs) and Non-Ideal Solutions (NISs). As shown, multiple optimal points are identified in the Pareto frontiers that describe the optimization curve achieved in the multi-criterion evaluation; the trend equations represent optimized functions for the calculation of the indicators based on other exergetic parameters.

Table 11. Regression coefficients for objective functions.

Configuration with superheat						
	$\mathbf{a_1}$	$\mathbf{a_2}$	$\mathbf{a_3}$	$\mathbf{a_4}$	$\mathbf{a_5}$	**k**
Min EWR	-1.69×10^{-4}	-1.15×10^{-5}	3.44×10^{-5}	3.86×10^{-3}	3.29×10^{-7}	0.885
	$\mathbf{b_1}$	$\mathbf{b_2}$	$\mathbf{b_3}$	$\mathbf{b_4}$	$\mathbf{b_5}$	**k**
Min EEF	-1.44×10^{-3}	3.41×10^{-4}	-1.98×10^{-3}	-5.50×10^{-3}	2.76×10^{-6}	3.536
Configuration with superheat and recompression						
	$\mathbf{a_1}$	$\mathbf{a_2}$	$\mathbf{a_3}$	$\mathbf{a_4}$	$\mathbf{a_5}$	**k**
Min EWR	-4.36×10^{-4}	-7.56×10^{-7}	2.94×10^{-5}	2.94×10^{-3}	7.13×10^{-4}	0.758
	$\mathbf{b_1}$	$\mathbf{b_2}$	$\mathbf{b_3}$	$\mathbf{b_4}$	$\mathbf{b_5}$	k
Min EEF	-6.64×10^{-4}	1.87×10^{-3}	-1.18×10^{-2}	-5.96×10^{-2}	1.24×10^{-6}	3.336

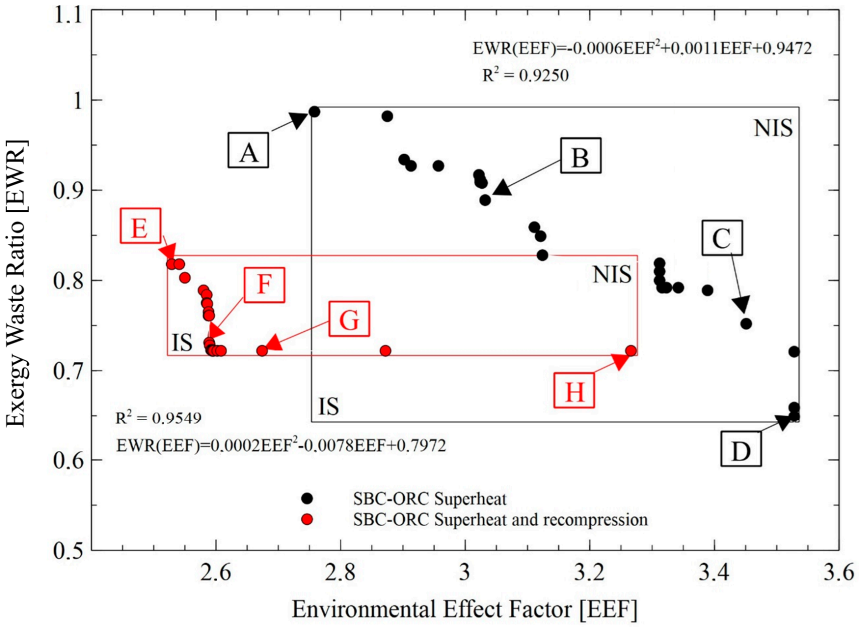

Figure 13. Pareto frontiers EWR with EEF for each configuration.

The optimal points selected represent the result of the optimization, where four criteria were taken in the face of different variations described in the sensitivity analyses to obtain the configuration of optimal values that seeks to minimize the amount of exergy destroyed while the exergy indicators decrease without affecting the first-law efficiency, second-law efficiency, and net power of the system. The points shown in the figure are presented below with the values that constitute them for both configurations, Table 12.

Table 12. Optimum values of criteria and objective functions.

Point	T_1	AP	r_p	ex_{dest}	EWR	EEF
Configuration with superheat						
ref	800	39	15	397.356	0.989	3.312
A	801.000	23.338	11.000	397.356	0.987	2.758
	742.000	29.879	6.000	395.329	0.927	2.957
B	616.000	41.593	7.000	392.250	0.889	3.032
	839.000	42.020	8.000	418.952	0.810	3.312
C	711.000	44.892	7.000	360.321	0.721	3.528
	607.000	24.801	6.000	365.887	0.649	3.528
D	615.000	38.811	4.000	463.915	0.427	3.528

Table 12. *Cont.*

Point	T_1	AP	r_p	ex_{dest}	EWR	EEF
Configuration with superheat and recompression						
ref	800	39	9	372.379	0.761	2.602
E	600.000	20.000	2.000	340.000	0.818	2.529
	684.000	31.760	7.000	478.615	0.789	2.580
F	624.000	43.513	8.000	352.044	0.731	2.592
	746.000	35.305	5.000	501.661	0.722	2.596
G	791.000	23.522	5.000	380.782	0.722	2.675
	718.000	31.942	6.000	399.535	0.722	3.266
H	695.000	40.900	3.000	392.555	0.722	3.266

Using TOPSIS Equations (31)–(33), the distances between points concerning their reference are calculated to obtain the optimum point of the optimization problem. Point F is the ideal point since it is closer to the IS and farther from the NIS. At the same time, it guarantees the minimum amount of total exergy destroyed in the overall system, Table 13.

Table 13. Optimal multi-objective solution.

Optimal Point	Objective Functions		C1	C2	C3	C4
	EWR	EEF	T_1	AP	r_p	ex_{dest}
F	0.731	2.592	624 °C	43.5 °C	8	352 kW

The optimum point guarantees a value of 2.59 and 0.73 in the environmental effect factor (EEF) and exergy–waste ratio (EWR). This implies a reduction of 6.04%, 14.53%, 24.94%, and 26.60% in the EEF when comparing the optimum point with configurations A, B, C, and D of the combined cycle with superheat (see Figure 13). In the case of the EWR, reductions of 25.81%, 17.37%, and 1.84% were evidenced when compared to configurations A, B, and C. For the combined cycle with superheat and recompression, it was observed that the optimum configuration allows a reduction in the EEF of 3.02% and 20.72% when compared to configurations G and H. Also, a reduction of 10.67% in the EWR was witnessed when compared to configuration E.

4. Conclusions

As a result of the increase in national and global energy demand, the environmental impact caused by the exploitation of conventional resources has caused irreparable damage. To help mitigate the negative effects that this can have on society, there has been an increase in the research needed to take advantage of energy sources with a lesser environmental impact. The environmental analysis indicates that the burner is the main component with the most significant environmental exergy impact, with a share of 27.06%. The solar tower is the main source of exergy destroyed in the combined cycle with a value of 212.23 kW, representing 52.77% of the total exergy destroyed. Thermal irreversibilities due to high-temperature gradients are one of the main reasons for this behavior.

From the correlation analysis, it could be observed that the selected study variables have a high linear relationship with respect to the selected performance parameters; however, when analyzing the relationship of the turbine inlet temperature, for the first-law efficiency, the second-law efficiency, and the environmental indices EWR, EEF, and ESI, although it influences the output parameters, this relationship is not completely linear. Although EEF and ESI influence the output parameters, this relationship is not completely linear.

For high temperatures, in general, higher first-law efficiency and power generation were achieved; but at very high temperatures, the second-law efficiency was somewhat lower when compared to the effect on the other study variables. Most of the exergetic losses were in the heat transfer devices, which increases the losses in this type of device and is the implicit energy loss that requires a heat transfer process and demonstrates the difficulty of matching the temperature profile between working fluids. The exergetic efficiency of a system can be increased using a suitable working fluid; in past studies, it was found that the use of mixtures can significantly improve the efficiency of these power generation systems. The inlet turbine temperature correlates positively with important performance variables in the combined cycle, such as net power generation (W_net) and total destroyed exergy (Edtotal).

The multi-objective optimization was crucial to determine the ideal performance parameters for the performance of the overall system and the proper use of the exergy present in the equipment and in the working fluids that interact with each other; in favor of this situation, the optimal result indicated that the water and air streams that pass through the condenser and the cooler, respectively, are sources of exergy destruction due to the low use of this energy in the system with simple superheat. Thus, it was observed that in using the system with recompression, the temperatures in the system are distributed in a better way due to the inclusion of the LTR, which minimizes the exergy destruction and favors the measurements with the exergy and environmental exergy indicators. Also, it was concluded that the temperature in base conditions is not appropriate with 800 °C but with 624 °C to guarantee the efficiencies and reduce the losses in the hybrid system.

The optimum point found in the research allows for the reaching of values of 2.59 and 0.73 in the environmental effect factor (EEF) and the exergy–waste ratio (EWR). In general, the optimization process proposed in the research allows for reducing the environmental effect factor (EEF) by between 3.02% and 26.60% and the exergy–waste ratio (EWR) by between 1.84% and 25.81%.

Author Contributions: Conceptualization: G.V.-O.; Methodology: G.V.-O. and J.D.-F.; Software: G.V.-O., J.D.-F. and D.M.-C.; Validation: G.V.-O., J.D.-F. and D.M.-C.; Formal Analysis: G.V.-O., J.D.-F. and D.M.-C.; Investigation: G.V.-O.; Resources: G.V.-O.; Writing—Original Draft Preparation: G.V.-O. and J.D.-F.; Writing—Review and Editing: J.D.-F. and D.M.-C.; Funding Acquisition: G.V.-O. All authors have read and agreed to the published version of the manuscript.

Funding: This research received no external funding.

Data Availability Statement: The data used were specified in the manuscript.

Acknowledgments: Acknowledgments to Universidad del Atlántico for the support received through the project ING712-CII2023 to conduct this research.

Conflicts of Interest: The authors declare no conflicts of interest.

Abbreviations

The following abbreviations are used in this manuscript:

Nomenclature

Abbreviation	
HR	Heater
HTR	High-Temperature Recuperator
LTR	Low-Temperature Recuperator
NIS	Negative Ideal Solution
ORC	Organic Rankine Cycle
PCHE	Printed Cycle Heat Exchanger
PIS	Positive Ideal Solution
RHR	Re-Heater

SBC	Supercritical Brayton Cycle
Symbols list	
EHR	Exhaust heat recovery
e	Exergy
h	Enthalpy
I	Environmental impact
$\dot{m}$	Mass flow
P	Pump
T	Temperature
Q	Heat
W	Work
X_i	Mole fraction
Greek letters	
η	Efficiency
Subscripts	
dest	Destroyed exergy

References

1. Ghadikolaei, R.S.; Manesh, M.H.K.; Modabber, H.V.; Onishi, V.C. Thermo-environ-economic optimization of an integrated combined-cycle power plant based on a multi-objective water cycle algorithm. *Iran. J. Sci. Technol. Trans. Mech. Eng.* **2024**, *48*, 439–460. [CrossRef]
2. Okati, V.; Moghadam, A.J.; Farzaneh-Gord, M.; Moein-Jahromi, M. 4E and Multi-criteria Optimization of a New Alternative Intercooling Method for Modified Brayton Cycle on the Operation of a Hybrid Energy System. *Iran. J. Sci. Technol. Trans. Mech. Eng.* **2024**, *48*, 881–906. [CrossRef]
3. Bhardwaj, S.; Nair, K.; Tariq, M.U.; Ahmad, A.; Chitnis, A. The state of research in green marketing: A bibliometric review from 2005 to 2022. *Sustainability* **2023**, *15*, 2988. [CrossRef]
4. Thirunavukkarasu, M.; Sawle, Y.; Lala, H. A comprehensive review on optimization of hybrid renewable energy systems using various optimization techniques. *Renew. Sustain. Energy Rev.* **2023**, *176*, 113192. [CrossRef]
5. Li, W.; Zou, Y.; Yang, H.; Fu, X.; Li, Z. Two stage Stochastic Energy Scheduling for Multi Energy Rural Microgrids With Irrigation Systems and Biomass Fermentation. *IEEE Trans. Smart Grid* 2024, *early access*. [CrossRef]
6. Awan, M.M.A.; Asghar, A.B.; Javed, M.Y.; Conka, Z. Ordering technique for the maximum power point tracking of an islanded solar photovoltaic system. *Sustainability* **2023**, *15*, 3332. [CrossRef]
7. Kalogirou, S.A. Solar thermal collectors and applications. *Prog. Energy Combust. Sci.* **2004**, *30*, 231–295. [CrossRef]
8. Khan, Y.; Raman, R.; Rashidi, M.M.; Caliskan, H.; Chauhan, M.K.; Chauhan, A.K. Thermodynamic analysis and experimental investigation of the water spray cooling of photovoltaic solar panels. *J. Therm. Anal. Calorim.* **2023**, *148*, 5591–5602. [CrossRef]
9. Yang, Z.; Ren, Z.; Li, H.; Sun, Z.; Feng, J.; Xia, W. A multi-stage stochastic dispatching method for electricity-hydrogen integrated energy systems driven by model and data. *Appl Energy* **2024**, *371*, 123668. [CrossRef]
10. Zhang, L.; Liu, D.; Cai, G.; Lyu, L.; Koh, L.H.; Wang, T. An optimal dispatch model for virtual power plant that incorporates carbon trading and green certificate trading. *Int. J. Electr. Power Energy Syst.* **2023**, *144*, 108558. [CrossRef]
11. Lin, L.; Chen, C.; Wei, B.; Li, H.; Shi, J.; Zhang, J.; Huang, N. Residential electricity load scenario prediction based on transferable flow generation model. *J. Electr. Eng. Technol.* **2023**, *18*, 99–109. [CrossRef]
12. Khan, Y.; Mishra, R.S. Performance evaluation of solar based combined pre-compression supercritical CO2 cycle and organic Rankine cycle. *Int. J. Green Energy* **2021**, *18*, 172–186. [CrossRef]
13. Zhou, J.; Ali, M.A.; Zeki, F.M.; Dhahad, H.A. Thermoeconomic investigation and multi-objective optimization of a novel efficient solar tower power plant based on supercritical Brayton cycle with inlet cooling. *Therm. Sci. Eng. Prog.* **2023**, *39*, 101679. [CrossRef]
14. Khan, Y.; Singh, D.; Caliskan, H.; Hong, H. Exergoeconomic and Thermodynamic Analyses of Solar Power Tower Based Novel Combined Helium Brayton Cycle-Transcritical CO_2 Cycle for Carbon Free Power Generation. *Glob. Chall.* **2023**, *7*, 2300191. [CrossRef]
15. Khan, Y.; Apparao, D.; Gawande, S.; Singh, N.; Bisht, Y.S.; Singh, P. Performance Assessment and Working Fluid Selection of the Novel Combined Helium Brayton Cycle and Organic Rankine Cycle Based on Solar Power Tower for Sustainable Generation. *Iran. J. Sci. Technol. Trans. Mech. Eng.* **2024**, *48*, 1901–1916. [CrossRef]
16. Etghani, M.M.; Boodaghi, H. Design and performance assessment of a novel poly-generation system with stable production of electricity, hydrogen, and hot water: Energy and exergy analyses. *Arab. J. Sci. Eng.* **2024**, *49*, 10471–10499. [CrossRef]
17. Muralikrishna, K.; Shenoy, U.V. Heat exchanger design targets for minimum area and cost. *Chem. Eng. Res. Des.* **2000**, *78*, 161–167. [CrossRef]

18. Quoilin, S.; Aumann, R.; Grill, A.; Schuster, A.; Lemort, V.; Spliethoff, H. Dynamic modeling and optimal control strategy of waste heat recovery Organic Rankine Cycles. *Appl. Energy* **2011**, *88*, 2183–2190. [CrossRef]
19. Hou, S.; Li, H.; Zhang, H. Open air—Vapor compression refrigeration system for air conditioning and hot water cooled by cool water. *Energy Convers. Manag.* **2007**, *48*, 2255–2260. [CrossRef]
20. Matthew, O.; Nieh, S. Effects of ORC working fluids on combined cycle integrated with SOFC and ORC for stationary power generation. *Energy Power Eng.* **2019**, *11*, 167–185. [CrossRef]
21. Chammam, A.; Tripathi, A.K.; Alvarez, J.R.N.; Alsaab, H.O.; Romero-Parra, R.M.; Mayet, A.M.; Abdullaev, S.S. Multiobjective optimization and performance assessment of a PEM fuel cell-based energy system for multiple products. *Chemosphere* **2023**, *337*, 139348. [CrossRef] [PubMed]
22. Khaliq, A.; Refaey, H.A.; Alharthi, M.A. Development and analysis of a novel CSP source driven cogeneration cycle for the production of electric power and low temperature refrigeration. *Int. J. Refrig.* **2021**, *130*, 330–346. [CrossRef]
23. Sridharan, M. Performance augmentation study on a solar flat plate water collector system with modified absorber flow design and its performance prediction using the XGBoost algorithm: A machine learning approach. *Iran. J. Sci. Technol. Trans. Mech. Eng.* **2024**, *48*, 133–144. [CrossRef]
24. Observatorio del Caribe Colombiano. *Región Caribe Colombiana*; Observatorio del Caribe Colombiano: Cartagena de Indias, Colombia, 2015; Volume 25.
25. Castillo, Y.; Gutiérrez, M.C.; Vanegas-Chamorro, M.; Valencia, G.; Villicaña, E. Rol de las Fuentes No Convencionales de Energía en el sector eléctrico colombiano. *Prospectiva* **2015**, *13*, 39–51. [CrossRef]
26. Campos Avella, J.C.; Lora Figueroa, E.; Meriño, L.; Tovar, I.; Navarro, A.; Quispe, E.C.; Vidal, J.R.; Castrillón, Y.; Castrillón, R.; Prias, O. *Guía Para la Implementación de Sistemas de Gestión Integral de la Energía*; UPME, COLCIENCIAS: Bogota, Colombia, 2008.
27. Gómez Ramírez, J. *La Energía Solar Fotovoltaica en Colombia: Potenciales, Antecedentes y Perspectivas*; Universidad Santo Tomas: Bogotá, Colombia, 2017.
28. Etghani, M.M.; Shojaeefard, M.H.; Khalkhali, A.; Akbari, M. A hybrid method of modified NSGA-II and TOPSIS to optimize performance and emissions of a diesel engine using biodiesel. *Appl. Therm. Eng.* **2013**, *59*, 309–315. [CrossRef]
29. Babatunde, M.; Ighravwe, D. A CRITIC-TOPSIS framework for hybrid renewable energy systems evaluation under techno-economic requirements. *J. Proj. Manag.* **2019**, *4*, 109–126. [CrossRef]
30. American Burners. Quemadores a Biomasa. Available online: https://www.americanbiomasa.com.ar/assets/catbiomasa.pdf (accessed on 24 November 2024).
31. Cáceres-Martínez, L.E.; Guío-Pérez, D.C.; Rincón-Prat, S.L. Potencial energético teórico y técnico de biomasa residual disponible en Colombia para el aprovechamiento en procesos de transformación termoquímica. In Proceedings of the Tercer Congreso de Energía Sostenible, Bogotá, Colombia, 24–26 October 2016; pp. 106–111.
32. Ge, Z.; Li, J.; Duan, Y.; Yang, Z.; Xie, Z. Thermodynamic performance analyses and optimization of dual-loop organic Rankine cycles for internal combustion engine waste heat recovery. *Appl. Sci.* **2019**, *9*, 680. [CrossRef]
33. Franchetti, B.; Pesiridis, A.; Pesmazoglou, I.; Sciubba, E.; Tocci, L. Thermodynamic and technical criteria for the optimal selection of the working fluid in a mini-ORC. In Proceedings of the ECOS 2016, Portorož, Slovenia, 19–23 June 2016.
34. Koç, Y. Parametric optimisation of an ORC in a wood chipboard production facility to recover waste heat produced from the drying and steam production process. *Energies* **2019**, *12*, 3656. [CrossRef]
35. Michos, C.N.; Lion, S.; Vlaskos, I.; Taccani, R. Analysis of the backpressure effect of an Organic Rankine Cycle (ORC) evaporator on the exhaust line of a turbocharged heavy duty diesel power generator for marine applications. *Energy Convers. Manag.* **2017**, *132*, 347–360. [CrossRef]
36. Tovar, J.M.; Ochoa, G.V.; Casseres, D.M. Thermodynamic and environmental comparative analysis of a dual loop ORC and Kalina as bottoming cycle of a solar Brayton sCO_2. *Int. J. Thermofluids* **2024**, *24*, 100895. [CrossRef]
37. Padilla, R.V.; Soo Too, Y.C.; Benito, R.; Stein, W. Exergetic analysis of supercritical CO_2 Brayton cycles integrated with solar central receivers. *Appl. Energy* **2015**, *148*, 348–365. [CrossRef]
38. Fontalvo, A. Análisis Termoeconómico de la Aplicación de un Ciclo Rankine Orgánico Para Aprovechamiento de Calor de Desecho de Baja Temperatura. Master's Thesis, Universidad del Norte, Barranquilla, Colombia, 2015. Available online: https://manglar.uninorte.edu.co/handle/10584/10728 (accessed on 24 January 2024).
39. Kamari, M.L.; Maleki, A.; Daneshpour, R.; Rosen, M.A.; Pourfayaz, F.; Nazari, M.A. Exergy, energy and environmental evaluation of a biomass-assisted integrated plant for multigeneration fed by various biomass sources. *Energy* **2023**, *263*, 125649. [CrossRef]
40. Zhu, Y.; Zhai, R.; Peng, H.; Yang, Y. Exergy destruction analysis of solar tower aided coal-fired power generation system using exergy and advanced exergetic methods. *Appl. Therm. Eng.* **2016**, *108*, 339–346. [CrossRef]